16 P-T-a(H_2O) Conditions in the Thermal Aureole

D.R.M. Pattison

16.1 Introduction

In this chapter estimates are made of the pressure of emplacement of the Ballachulish Igneous Complex and the range of maximum temperatures in the surrounding thermal aureole. Using these P-T estimates, quantitative estimates of a(H_2O) are made for pelites at different grades in the aureole. Activity of H_2O is shown to vary between pelites above and below the onset of partial melting, and between graphitic and non-graphitic pelites at the same grade.

The first part of the chapter summarizes a quantitative calibration by Pattison (1989) of the well-defined sequence of pelitic reactions in the aureole (Pattison and Harte, Chap. 8, this Vol.). P-T estimates from calibrated geothermometers and geobarometers (Pattison 1989), carbonate reactions (Masch and Heuss-Aβbichler, Chap. 10, this Vol.), microcline-sanidine transformation (Kroll et al., Chap. 13, this Vol.) and late-stage haplogranites in the igneous complex (Weiss and Troll, Chap. 4, this Vol.) are used to constrain further P-T conditions in the aureole. Four thermal profiles, including ones across the widest and narrowest parts of the aureole, are constructed to constrain the thermal modelling of Buntebarth (Chap. 18, this Vol.).

Quantitative estimates of a(H_2O) show that dehydration reactions occur at lower temperatures and melting reactions occur at higher temperatures in graphitic pelites compared to non-graphitic units. Lowered a(H_2O) accounts for several conspicuous features of assemblages in the graphitic Ballachulish Slate, such as the development of incipient cordierite farther from the igneous contacts in the Ballachulish Slate than in the other non-graphitic pelitic units, the exclusive development of andalusite-bearing assemblage IVa in the Ballachulish Slate, and the anomalously magnesian compositions of cordierite and biotite in assemblage IVa compared to assemblages in non-graphitic units (Pattison and Harte, Chap. 8, this Vol.).

In the zone of partial melting, variation in a(H_2O) is assessed by the construction of a semi-quantitative T-a(H_2O) diagram. It is argued that melting reactions internally buffered a(H_2O) to low values as melting proceeded. Prograde paths for the most common pelitic and semipelitic assemblages are discussed with reference to melting reactions in the T-a(H_2O) diagram.

The chapter closes with a short discussion of the importance of equilibrium and kinetics in controlling the distribution and chemical composition of pelitic assemblages in the aureole. Most of the evidence suggests that gross equilibrium prevailed during contact metamorphism, although kinetic effects are in evidence in

G. Voll, J. Töpel, D.R.M. Pattison, F. Seifert
Equilibrium and Kinetics
in Contact Metamorphism

16.8 Summary

Calibration of the pelitic reactions mapped around the Ballachulish Igneous Complex allows an assessment of the pressure of emplacement of the igneous complex and variation in temperature in the thermal aureole. Additional constraints are provided from geothermometry and geobarometry of high grade pelitic assemblages, calibrated carbonate reactions, calcite-dolomite geothermometry, and the microcline-sanidine transformation.

Four independent methods of calculating pressure range between 2.8 and 3.2 kbar, resulting in a best estimate of 3.0 ± 0.5 kbar. Selected maximum temperatures in the aureole include: 370–480 °C for the growth of talc by reaction (C1); 470–490 °C for the transformation of microcline to sanidine; 550 and 560 °C for the first appearance of cordierite [reaction (P1)] in graphitic and non-graphitic pelites, respectively; 620 °C for isobaric invariant assemblage CIII (Fo + Tr + Di + Cc + Dol); 625 and 640 °C for Ms + Qtz = Al_2SiO_5 + Kfs + H_2O [reaction (P3)] in graphitic and non-graphitic pelites, respectively: 670 °C for the onset of migmatisation in non-graphitic, plagioclase-bearing pelites; 750 °C for the formation of garnet in high grade pelites; and 750–800 °C for the formation of hypersthene in high grade pelites and periclase in dolomitic marbles. From these estimates, the maximum contact tempera-

ture is estimated to have been 750–800 °C. Four thermal profiles were constructed across different parts of the thermal aureole, including the narrowest and widest parts; these are used to constrain the thermal models of Buntebarth (Chap. 18, this Vol.).

In graphitic pelites such as the Ballachullish Slate, the interaction of graphite with the predominantly hydrous fluid resulted in the addition to the fluid of C-bearing species such as CH_4 and CO_2. The presence of C-bearing fluid species shifted a(H_2O) to lower values, resulting in the onset of pelitic dehydration reactions at lower temperatures and vapour-consuming melting reactions at higher temperatures in graphitic pelites compared to adjacent non-graphitic pelites. Lowered a(H_2O) expanded the stability field of andalusite-bearing assemblage IVa [reaction (P2a)], thereby explaining the restriction of this assemblage to the Ballachulish Slate. The shift in stability of reaction (P2a) also accounts for the anomalously magnesian compositions of cordierite and biotite in assemblage IVa.

With the onset of partial melting, all available free water was consumed. Further melting proceeded at reduced a(H_2O), with the melting reactions internally buffering a(H_2O) to lower values as melting proceeded. The highest grade pelitic assemblage, Grt + Hy + Crd + Bt, records a(H_2O) of about 0.2 at 760 °C. Prograde paths of the most common pelitic and semipelitic assemblages along a(H_2O)-buffering melting reactions are illustrated in a semi-quantitative T-a(H_2O) diagram.

The regular distribution of pelitic assemblages in the aureole, and the consistency between predicted and measured mineral compositions going through a sequence of continuous reactions, suggest that gross equilibrium prevailed during metamorphism of the pelites. There is no evidence for overstepping of experimentally-determined reactions involving cordierite.

Based on the first occurrence of sillimanite at the reaction (P3) isograd, the position of the And = Sil curve in P-T space is constrained to lie between the And = Sil curves of Richardson et al. (1969) and Holdaway (1971). Persistence of andalusite well upgrade of the first occurrence of sillimanite is ascribed to the sluggish kinetics of the polymorphic inversion reaction, which may have been controlled by the availability of fluid.

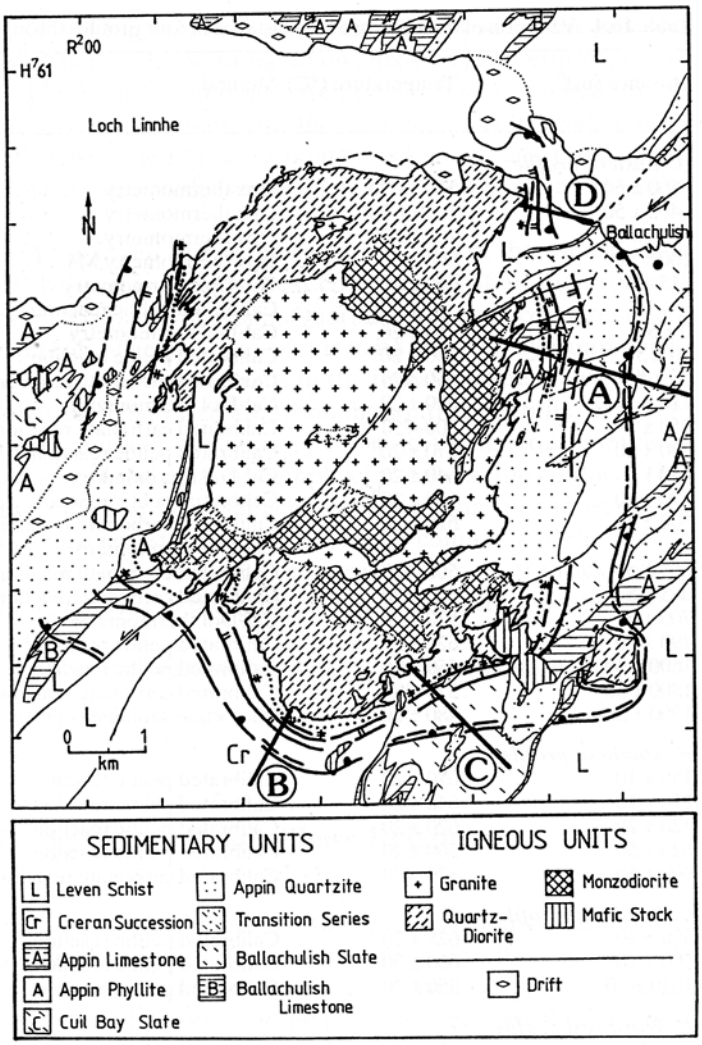

Fig. 16.4. Location of the four thermal profiles illustrated in Figs. 16.5–16.8

16.4.5 Temperature Profiles in the Aureole

Using all of the temperature estimates from the above equilibria, four thermal profiles were constructed across different parts of the thermal aureole (see Figs. 16.4–16.8). The most widely applicable method of constraining the thermal profiles is the series of calibrated subsolidus pelitic reactions, which have been located around the whole igneous complex. Table 16.4 lists the distances, temperatures and methods used to construct the thermal profiles. Uncertainties in temperature and distance from the contact are from the authors of the different methods.

Table 16.4. Variation of temperature with distance in four profiles through the Ballachulish aureole

Distance (m)[a]	Temperature (°C)	Method	Reaction number or sample
A. Eastern profile			
–500 ± 50	1100 ± 70	Opx thermometry	M1[c]
–400 ± 50	1050 ± 70	Opx thermometry	M2
–250 ± 50	1020 ± 70	Opx thermometry	M3
100 ± 50	800 ± 60	Opx thermometry M4	
–15 ± 5	760 ± 20	Grt-Opx thermometry	DP568[d]
		Calibrated pelitic reaction	P12[e]
0 ± 5	760 ± 20	Cal-Dol thermometry	C(375)[f]
10 ± 5	750 ± 20	Calibrated pelitic reaction	P11
70 ± 5	650–970	Calibrated carbonate reaction	C15[g]
110 ± 5	680 ± 20	Cal-Dol thermometry	C(315)
350 ± 5	500–750	Calibrated carbonate reaction	C14
380 ± 20	670 ± 20[b]	Calibrated pelitic reaction	P5
450 ± 5	640 ± 20	Cal-Dol thermometry	C(309)
490 ± 10	640 ± 20[b]	Calibrated pelitic reaction	P3
500 ± 5	620 ± 20[b]	Calibrated carbonate reaction	CIII[g]
		Cal-Dol thermometry	C(307)
665 ± 5	500–620	Calibrated carbonate reaction	C10
685 ± 5	500–620	Calibrated carbonate reaction	C9
700 ± 5	530 ± 20	Cal-Dol thermometry	C(223)
790 ± 20	620 ± 20[b]	Calibrated pelitic reaction	P2b
1600 ± 50	550 ± 20[b]	Calibrated pelitic reaction	P1
1800 ± 50	370–480	Calibrated carbonate reaction	C1
1900 ± 50	480 ± 20[b]	Microcline-sanidine transition	—
B. Southern profile			
150 ± 10	670 ± 20	Calibrated pelitic reaction	P5
210 ± 10	640 ± 20	Calibrated pelitic reaction	P3
320 ± 20	620 ± 20	Calibrated pelitic reaction	P2b
620 ± 50	560 ± 20	Calibrated pelitic reaction	P1
900 ± 50	370–480	Calibrated carbonate reaction	C1
C. Southeast profile			
350 ± 30	625 ± 20	Calibrated pelitic reaction	P3
500 ± 20	600 ± 30	Calibrated pelitic reaction	P2a
1050 ± 50	550 ± 20	Calibrated pelitic reaction	P1
D. Northeast profile			
60 ± 5	670 ± 20	Calibrated pelitic reaction	P5
80 ± 5	640 ± 20	Calibrated pelitic reaction	P3
140 ± 10	620 ± 20	Calibrated pelitic reaction	P2b
340 ± 30	560 ± 20	Calibrated pelitic reaction	P1

[a]Negative distances are distances from contact *in the igneous complex*; positive distances are distances from the contact *in the country rocks*.
[b]Most reliable estimates in the eastern profile (see text for discussion of methods). Pressure in all profiles is assumed to be 0.3 GPa.
[c]Ml, etc. Magmatite sample from Weiss and Troll (Chap. 4, this Vol.).
[d]DP568, Metapelite sample from Pattison and Harte (Chap. 8, this Vol.).
[e]P12, etc., Pelitic reaction number (Pattison and Harte, Chap. 8, this Vol.).
[f]C(375), etc., Carbonate sample from Masch and Heuss-Aβbichler (Chap. 10, this Vol.).
[g]CIII and C15 etc., Isobaric invariant point and univariant reactions from Masch and Heuss-Aβbichler (Chap. 10, this Vol.).

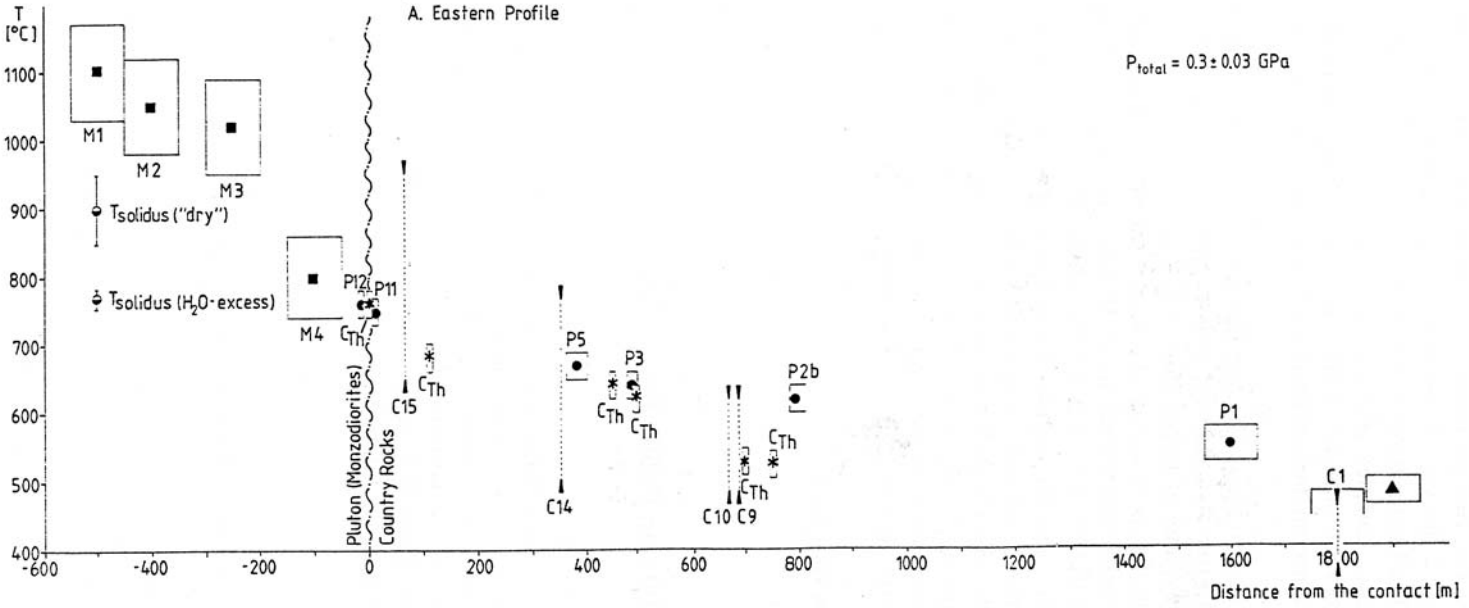

Fig. 16.5. East profile, taken across the widest part of the aureole. *Black dots* represent best estimate temperatures and locations for pelitic reactions (P1), (P2b), etc., with *boxes* representing uncertainties in temperature and location; the same convention is adopted for *filled squares* and surrounding *boxes* (magmatic temperatures, Weiss and Troll, Chap. 4, this Vol.), *stars* and *surrounding boxes* (calcite-dolomite geothermometry, Masch and Heuss-Aβbichler, Chap. 10, this Vol.) and *triangle*and *surrounding box* (microcline-sanidine transformation, Kroll et al. Chap. 13, this Vol.). *Inverted pointed triangles* connected by *dotted lines* represent the temperature limits of $X(CO_2)$-dependent carbonate reactions (C1), (C6), etc. (Masch and Heuss-Aβbichler, Chap. 10, this Vol.).

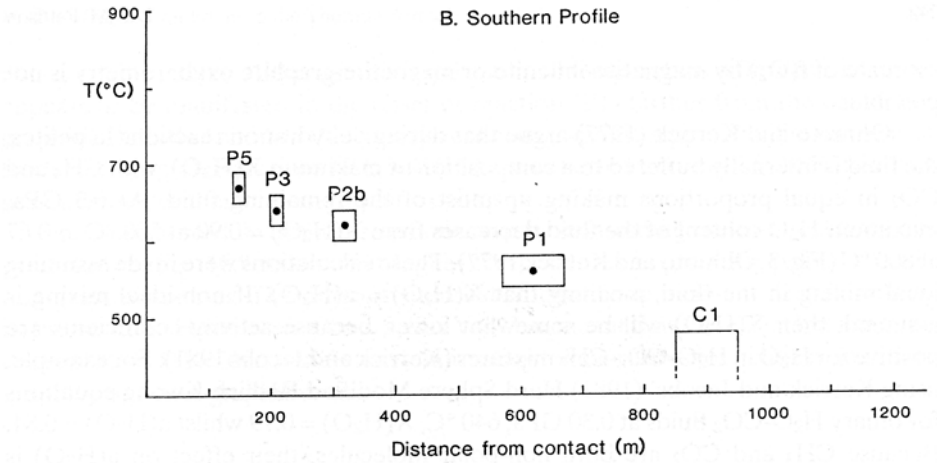

Fig. 16.6. Southern profile. All *symbols* as in Fig. 16.4

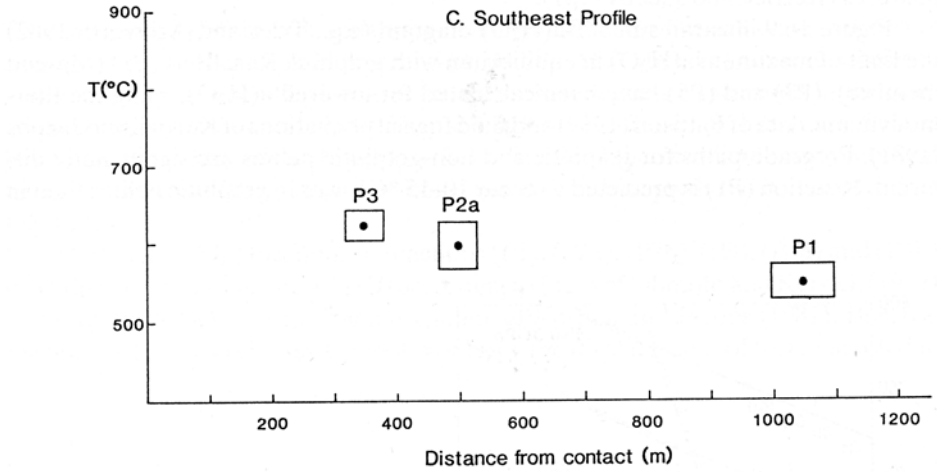

Fig. 16.7. Southeast profile. all *symbols* as in Fig. 16.4

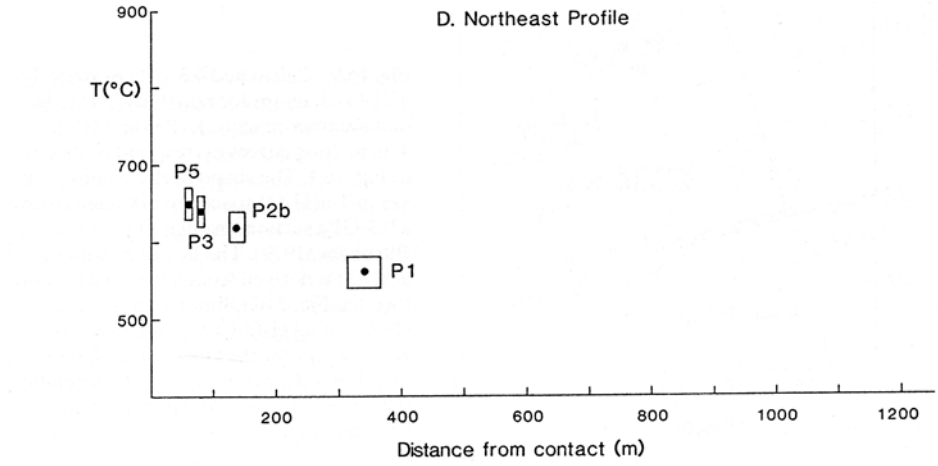

Fig. 16.8. Northeast profile, taken across the narrowest part of the aureole. All *symbols* as in Fig. 16.4

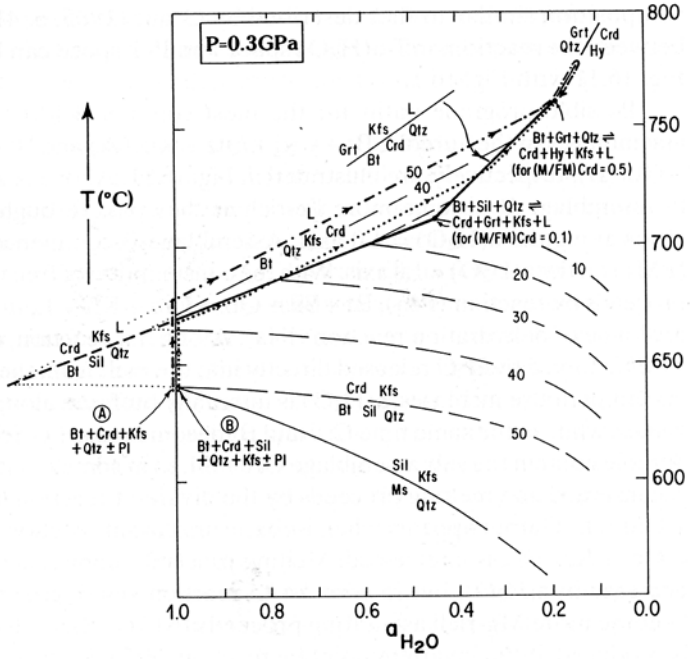

Fig. 16.11. Semi-quantitative 0.3-GPa isobaric T-a(H_2O) diagram for pelites in the zone of partial melting. Reactions (P3) (Ms + Qtz + Kfs + Sil + H_2O) and (P4a) (Bt + Sil + Qtz = Crd + Kfs + H_2O) are calculated from the thermodynamic data of Pattison (1989). *Dashed lines* with *numbers* are isopleths of Mg/(Mg + Fe) in cordierite for reaction (P4a). See text for discussion

compositions of biotite, hypersthene and K-feldspar are $K_{0.87}Na_{0.04}Mg_{0.87}Fe_{1.49}Ti_{0.30}Al_{1.44}Si_{2.71}O_{10}(OH)_2$, $Mg_{0.33}Fe_{0.63}Mn_{0.01}Al_{0.06}Si_{0.96}O_3$, and $K_{0.80}Na_{0.19}Ca_{0.01}Al_{1.02}Si_{2.98}O_8$. Activity models and resultant activities are:

$$a^{Hy}_{MgSiO_3} = \left(a^{Hy}_{Mg_2Si_2O_6}\right)^{1/2} = \left(X^{M_2}_{Mg} M^{M1}_{Mg}\right)^{1/2} = 0.345$$

$$a^{Bt}_{KMg_3AlSi_3O_{10}(OH)_2} = 9.48\left[X^{A}_{K} \bullet \left(X^{M}_{Mg}\right)^3 \bullet \left(X^{IV}_{Al}\right) \bullet \left(X^{IV}_{Si}\right) \bullet \left(X_{OH}\right)^2\right]$$

$$= 0.021 \quad (1)$$

$$or \quad = (X^{M}_{Mg})^3 = 0.030 \quad (2)$$

$$a^{Kfs}_{KAlSi_3O_8} = X^{A}_{K} = 0.80$$

Activity of SiO_2 in quartz is assumed to be 1.0. The resultant values of a(H_2O) are 0.18 (first biotite activity model) and 0.25 (second activity model); an a(H_2O) of 0.2 has been used in Fig. 16.11.

Between the 670 °C point on the a(H_2O) = 1.0 axis and the 760 °C, a(H_2O) = 0.2 point, the other reactions have been drawn in to be consistent with Fig. 16.1. Although plagioclase is present in many assemblages, for simplicity the reactions below just consider KFMASH phases. The melt phase is assumed to have a